ADVANCED FUNCTIONAL MATERIALS

Supporting Information

for *Adv. Funct. Mater.,* DOI: 10.1002/adfm.202204825

Impact of Hole-Transport Layer and Interface Passivation on Halide Segregation in Mixed-Halide Perovskites

*Vincent J.-Y. Lim, Alexander J. Knight, Robert D. J. Oliver, Henry J. Snaith, Michael B. Johnston, and Laura M. Herz**

Supporting Information: Impact of Hole-Transport Layer and Interface Passivation on Halide Segregation in Mixed-Halide Perovskites

Vincent J.-Y. Lim,[†] Alexander J. Knight,[†] Robert D. J. Oliver,[†] Henry J. Snaith,[†] Michael B. Johnston,[†] and Laura M. Herz[*,†,‡]

[†]*Department of Physics, University of Oxford, Clarendon Laboratory, Parks Road, Oxford, OX1 3PU, UK*

[‡]*Institute for Advanced Study, Technical University of Munich, Lichtenbergstrasse 2a, D-85748 Garching, Germany*

E-mail: laura.herz@physics.ox.ac.uk

Contents

1 Absorption Measurements

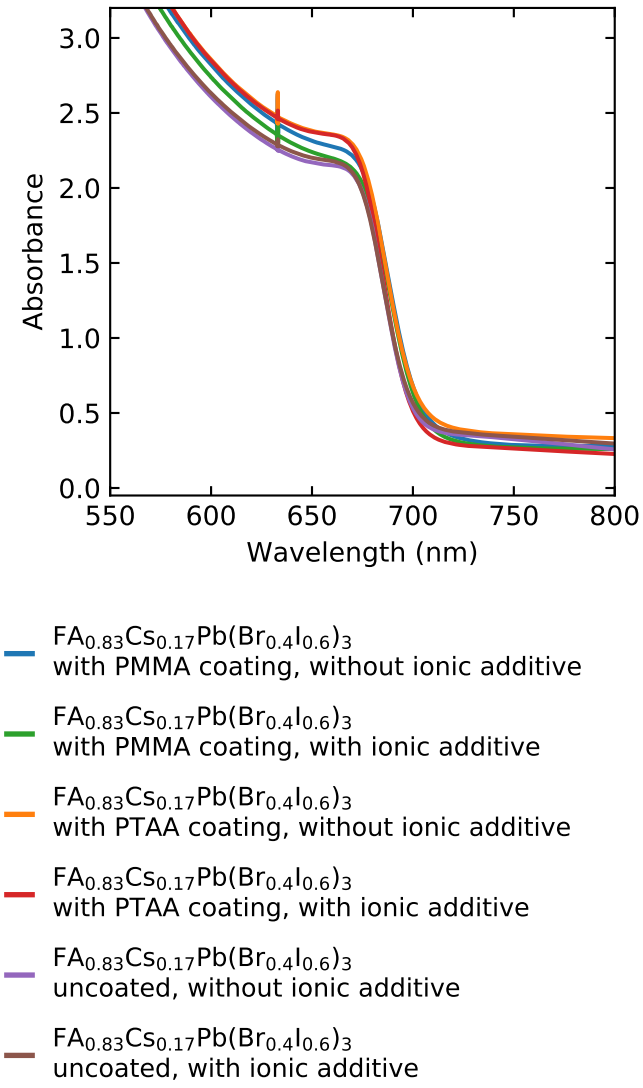

Supplementary Figure S1: Absorbance spectra for $FA_{0.83}Cs_{0.17}Pb(Br_{0.4}I_{0.6})_3$ thin films, top-coated with PMMA or PTAA, or uncoated, and with or without piperidinium ionic additive to the MHP, measured before any halide segregation may have occurred.

The absorption spectra of six sample combinations, resulting from $FA_{0.83}Cs_{0.17}Pb(Br_{0.4}I_{0.6})_3$ films made with or without piperidinium ionic salt, and with three options of either PMMA, PTAA or no top-layer coating are presented in Figure S1. Figure S1 shows that the six films exhibit very similar absorbance spectra, implying that neither top coating nor the piperidinium additive change the intrinsic absorption behavior of the $FA_{0.83}Cs_{0.17}Pb(Br_{0.4}I_{0.6})_3$

metal halide perovskite (MHP). The peaks at 632.8 nm are from He-Ne laser used for alignment within the FTIR.

2 In-Situ XRD/PL Measurements

We note that in previous experiments we showed that $MAPb(Br_{0.5}I_{0.5})_3$, known to be less stable than FACs-based MHPs, exhibited no damage under continuous X-ray illumination under the dark, even after a prolonged exposure for 18 hours.[S1]

All of the combined XRD/PL measurements were performed over 5 hours. Each of the XRD scans lasted 450 seconds, and the illumination source was only turned on after the first XRD scan had finished to ensure the first XRD scan is representative of the mixed-phase pristine state. The XRD/PL data presented are background corrected, and the PL data was further spectrally calibrated. To ensure the changes in the XRD patterns are caused by laser illumination, and that they correspond to a thin-film area for which the density of absorbed photons is relatively constant, the illumination spot size of the incident X-rays was much smaller than that of the exciting laser beam. The incident X-rays were collimated with a 2.5 degrees PB soller slit and 0.1mm collimator, and the full width half maximum of the two orthogonal axes of laser illumination were 1.2mm and 1.0mm. The centres of the two irradiation sources were aligned to each other and to the center of the thin-film sample 13mm-diameter substrate.

2.1 XRD/PL Data For Uncoated Films

Figure S3 presents the evolution of (220) XRD peak and PL spectra of uncoated $FA_{0.83}Cs_{0.17}Pb(Br_{0.4}I_{0.6})_3$ thin films, fabricated either with or without piperidinium ionic additive, under the same illumination conditions and recorded simultaneously. The PL and XRD evolutions of the uncoated films are qualitatively the same as those recorded for the equivalent PMMA-coated films (as seen in Figures 1 and 4 in the main text), but the PL spectra exhibited some

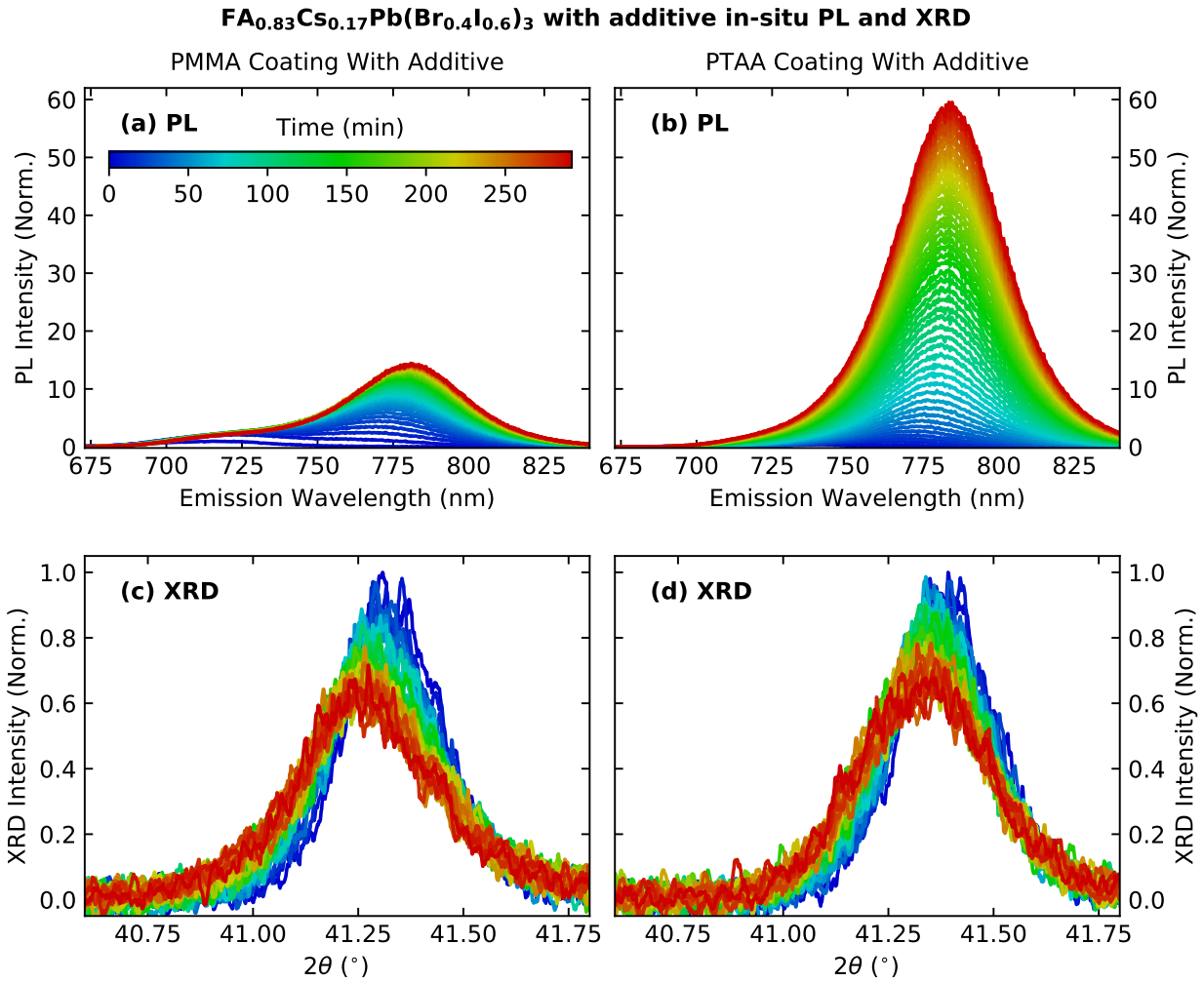

Supplementary Figure S2: Evolution under illumination (470 nm continuous wave (CW) illumination with 190 mW cm^{-2} intensity for $\sim$ 5 hours) of the PL spectra (top) and the second-order XRD peak recorded in-situ for uncoated $FA_{0.83}Cs_{0.17}Pb(Br_{0.4}I_{0.6})_3$ thin films with PMMA (left) and PTAA (right) coating with piperidinium ionic salt having been added during perovskite fabrication.

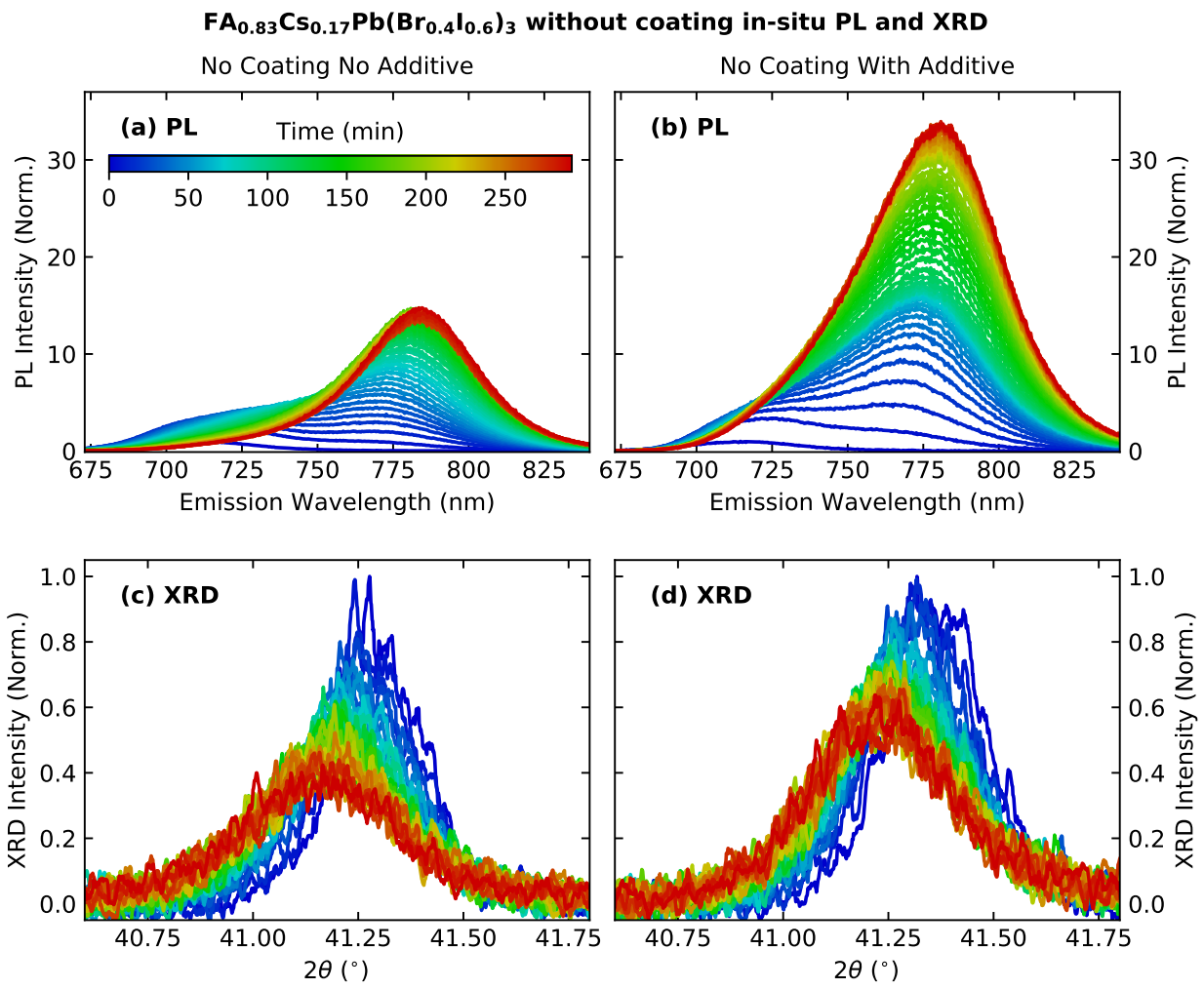

Supplementary Figure S3: Evolution under illumination (470 nm continuous wave (CW) illumination with 190 mW cm^{-2} intensity for $\sim$ 5 hours) of the PL spectra (top) and the second-order XRD peak recorded in-situ for uncoated $FA_{0.83}Cs_{0.17}Pb(Br_{0.4}I_{0.6})_3$ thin films without (left) and with (right) piperidinium ionic salt having been added during perovskite fabrication.

fluctuations, which we attribute to the MHP layer interacting with the ambient air, mainly oxygen.[S2–S5] The PL enhancement caused by the piperidinium ionic additive is still visible for these uncoated films.

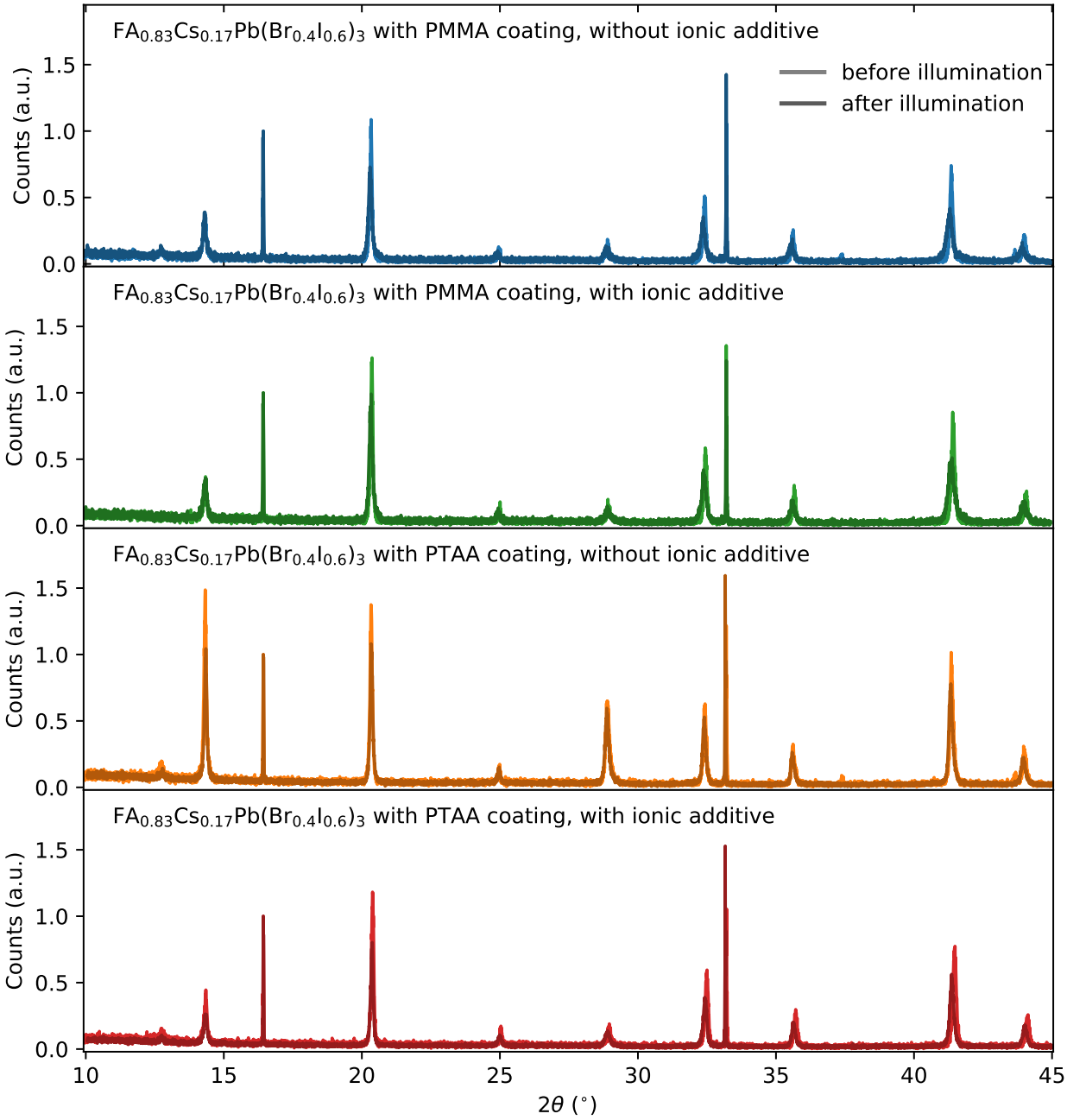

Supplementary Figure S4: Extended wide-angle XRD patterns of the four sample combinations under consideration, $FA_{0.83}Cs_{0.17}Pb(Br_{0.4}I_{0.6})_3$ thin films fabricated with or without piperidinium ionic additive and with either PTAA or PMMA top coating, recorded before and after the $\sim$ 5 hour illumination period for which halide segregation was investigated.

3 Wide-Angle XRD Patterns

A PANalytical X'Pert powder diffractometer with a Cu-$K_{\alpha 1}$ source across a 2θ range between 10° and 45° was used for wider XRD scans. Sample tilt was corrected for using the z-cut quartz substrate reference peak at $2\theta = 16.43°$ and applying a constant angular offset correction, and the the same peak at $2\theta = 16.43°$ was normalized to 1. XRD scans over a wider range were performed before and after illumination to check for any degradation. The results are presented in Figure S4, and it is evident that there are no non-perovskite peaks increasing in intensity or appearing after illumination, including the lack of growth of a PbI_2 peak at ∼12.8°. Another quartz peak at 33.2° appearing for each sample does not overlap perfectly before and after illumination, which is attributed to sample tilting which has not been fully compensated by the correction applied above.

4 Analysis of XRD Patterns

Bromide and iodide halide ions possess different ionic radii, so the bond length and therefore the lattice parameter of the MHP depends heavily on the halide content of the MHP, which is reflected in the XRD patterns by the Bragg equation. The MHP in its mixed-phase pristine state will possess narrow XRD peaks, corresponding to a narrow distribution of lattice parameters, indicating the homogeneous distribution of halide ions. Halide segregation will rearrange a fraction of halide ions within the bulk, and consequently iodide-rich and bromide-rich regions will form, presenting more extreme lattice parameters and therefore broadening the XRD peaks, as well as decreasing the maximum peak intensity and changing the shape of the XRD peaks. There are also several other factors that influence the shape of the XRD peaks. Firstly, the lattice spacing in the perovskite structure can be altered by strain, shifting the 2θ XRD angles, and this has previously been attributed to the decrease of peak XRD angle during halide segregation.[S6] Secondly, X-rays are known to be more sensitive to electron-rich ions, therefore iodide-rich regions will respond more strongly

to X-rays than bromide-rich regions, also decreasing the XRD angular position. Thirdly, perovskite degradation resulting in volume loss of perovskite structure can potentially affect the XRD peaks, although there was no significant degradation observed in the experiments conducted. Lastly, crystallinity and domain sizes can also alter the XRD peaks, affecting different regions to differing extent, which may also shift the XRD peak.

In the following sections, the XRD patterns acquired from in-situ XRD/PL measurements are further analysed.

4.1 XRD Peak Integral

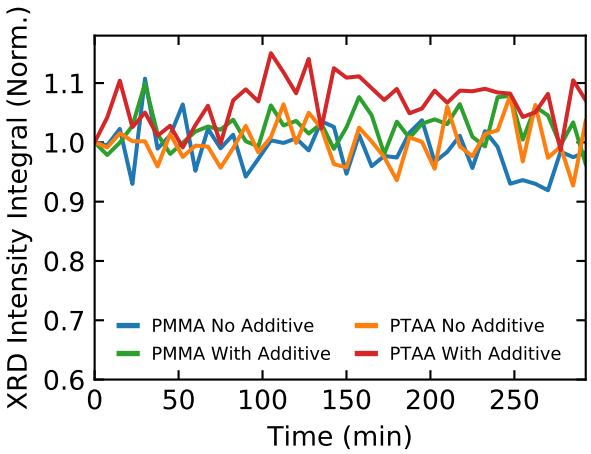

Supplementary Figure S5: The integrals across the (220) XRD peaks for the four sample combinations under consideration, $FA_{0.83}Cs_{0.17}Pb(Br_{0.4}I_{0.6})_3$ thin films fabricated with or without piperidinium ionic additive and with either PTAA or PMMA top coating, recorded during the $\sim$ 5 hour illumination period, and normalized to the initial integral before the start of the illumination cycle.

Figure S5 presents the integral of diffraction intensities across diffraction angles representing the pseudocubic (220) perovskite peak, as a function of the illumination time during halide segregation, for all four of the sample combinations under consideration. The integral range was between 40° and 42.5°, and the integrals for each of the films all remained constant over time, further corroborating the lack of degradation,[S1] and suggesting that the change

in the XRD peak is predominantly owing to a rearrangement of ions.

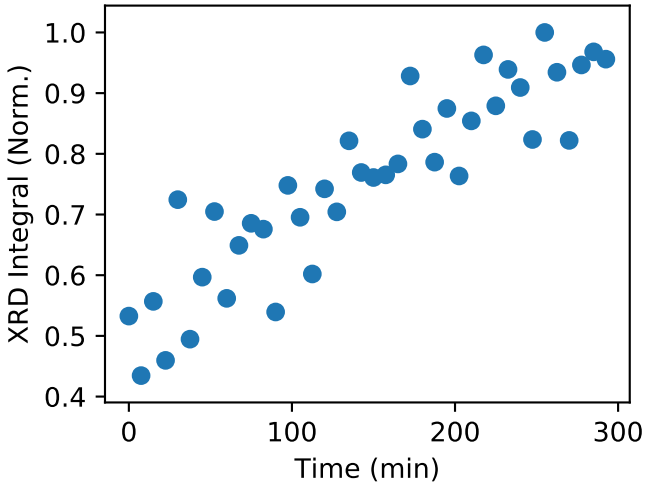

Supplementary Figure S6: The high-angle integrals across the (220) XRD peaks between 41.5° and 42° for the $FA_{0.83}Cs_{0.17}Pb(Br_{0.4}I_{0.6})_3$ thin film fabricated without piperidinium ionic additive and with PMMA top coating, recorded during the $\sim$ 5 hour illumination period, and normalized to the final integral at the end of the illumination cycle.

4.2 XRD Angle Change

Knight *et al.* recently examined the evolution of the XRD pattern to show that PMMA-coated methylammonium (MA)-based MHPs segregate differently to FACs-based MHPs.[S1] The XRD peak of $MAPb(Br_{0.5}I_{0.5})_3$ MHP decreased in amplitude as it underwent halide segregation, keeping the same central peak position. On the other hand, the XRD peak of $FA_{0.83}Cs_{0.17}Pb(Br_{0.4}I_{0.6})_3$ MHP, the same composition as investigated in this study, also decreased in amplitude during halide segregation, but the XRD peak shifted to lower angles while widening. The MA-based MHP also exhibited a growth in the tail regions of the XRD peak, further away from the central peak position. This was attributed to boundary-mediated halide segregation evolution, which does not affect the bulk of the MHP and therefore keeps the central peak position constant. In contrast to the lack of angle change in MA-based MHP, a bulk-mediated halide segregation in the FACs-based MHP affects the full volume of the material, causing a structural change throughout the MHP, shifting the XRD peak

angle.

As can be seen from Figure 1(d) in the main text, the PTAA-coated MHP without piperidinium additive does not show much, if any, angle change during the $\sim$ 5-hour illumination process. This lack of angle change is in contrast with the rest of the sample set, whose (220) XRD 2θ all decreased with halide segregation, and this decrease in angle is consistent with previous observations.[S1] Interestingly, this difference implies that upon the addition of piperidinium additive to a PTAA-coated MHP, its halide segregation behavior became comparable to that of PMMA-coated MHPs.

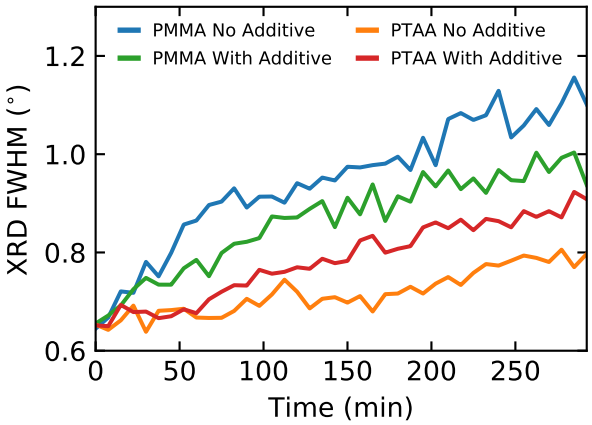

Supplementary Figure S7: Full width at half maximum of the (220) XRD peak angles for the four sample combinations under consideration $FA_{0.83}Cs_{0.17}Pb(Br_{0.4}I_{0.6})_3$ thin films fabricated with or without piperidinium ionic additive and with either PTAA or PMMA top coating, recorded during the $\sim$ 5 hour illumination period.

The 2θ XRD angle change is plotted in Figure S8 against the normalised XRD peak intensity of the (220) XRD peak for all sample combinations during the $\sim$ 5-hour illumination, clearly revealing different types of halide segregation behavior. The 2θ XRD angle and the XRD intensity were extracted through fits of a Gaussian function to each XRD pattern. The PTAA-coated MHP without piperidinium ionic additive shows a very constant 2θ XRD angle over illumination time, or even a very minor angle increase if there is any, and this is very similar to the boundary-mediated segregation dynamics observed in

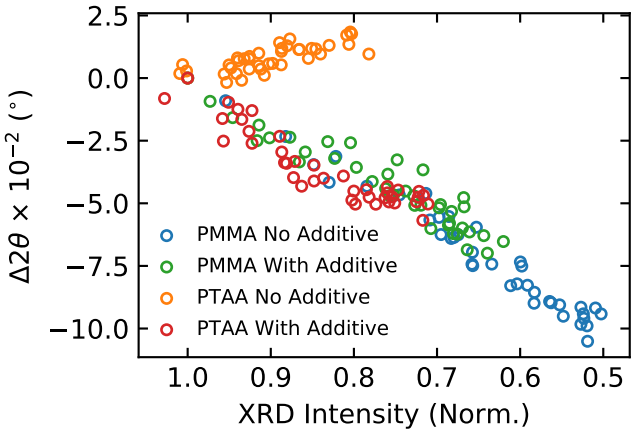

Supplementary Figure S8: The change in 2θ XRD angle, plotted against the peak amplitude of the (220) XRD peak for all four sample combinations under consideration, $FA_{0.83}Cs_{0.17}Pb(Br_{0.4}I_{0.6})_3$ thin films fabricated with or without piperidinium ionic additive and with either PTAA or PMMA top coating, recorded over the $\sim$ 5-hour illumination period.

the methylammonium-based MHP by Knight *et al.*[S1] This observation further corroborates the halide segregation dynamics in the PTAA-coated $FA_{0.83}Cs_{0.17}Pb(Br_{0.4}I_{0.6})_3$ film without piperidinium ionic additive occur only at the MHP-PTAA boundary. The other three samples, $FA_{0.83}Cs_{0.17}Pb(Br_{0.4}I_{0.6})_3$ with piperidinium ionic additive and PTAA coating, and both films with PMMA coating, qualitatively follow the same behavior (Figure S8). This similarity shows that a PTAA-coated MHP changes its halide segregation behavior to that of PMMA films upon the addition of piperidinium ionic additive, exhibiting a bulk-mediated halide segregation behavior. When piperidinium salt is added to $FA_{0.83}Cs_{0.17}Pb(Br_{0.4}I_{0.6})_3$ with PTAA coating, the trap states at the PTAA MHP interface are passivated.[S7] Although there is still expected to be some charge-carrier accumulation at the interface owing to Coulombic interaction, the lack of such interfacial trap states leads to a higher total charge-carrier population, on average and across the bulk, thereby causing halide segregation in the bulk as well.

5 PLQY Measurements

Photoluminescence quantum yield (PLQY) measurements were performed following the procedure reported by de Mello *et al.*[S8] and as reported by us previously.[S5,S9] In brief, the samples were placed in an integrating sphere and photoexcited by a 532 nm continuous wave laser. The photoluminescence was coupled into a fibre and collected by a QEPro spectrometer. The integrating sphere and fibre were calibrated using a lamp of known spectrum. The illumination intensity was 30 mW cm^{-2} which corresponds to approximately 0.5 suns equivalent absorbed photon flux[S10] at a bandgap of 1.6 eV, therefore the PLQY values presented here are underestimates of their value at one-sun equivalent conditions.

Table S1: PLQY measurements of uncoated and PTAA-coated $FA_{0.83}Cs_{0.17}Pb(Br_{0.4}I_{0.6})_3$ and $FA_{0.83}Cs_{0.17}Pb(Br_{0.1}I_{0.9})_3$ thin films with and without piperidinium ionic additive. (†) The PLQY data for $FA_{0.83}Cs_{0.17}Pb(Br_{0.4}I_{0.6})_3$ was taken from Oliver *et al.*[S11]

Sample Composition	Coating Layer	Ionic Additive	PLQY (%)
$FA_{0.83}Cs_{0.17}Pb(Br_{0.4}I_{0.6})_3$	Uncoated	No	0.221 †
$FA_{0.83}Cs_{0.17}Pb(Br_{0.4}I_{0.6})_3$	Uncoated	Yes	0.579 †
$FA_{0.83}Cs_{0.17}Pb(Br_{0.4}I_{0.6})_3$	PTAA	No	3.84×10^{-3} †
$FA_{0.83}Cs_{0.17}Pb(Br_{0.4}I_{0.6})_3$	PTAA	Yes	4.59×10^{-2} †
$FA_{0.83}Cs_{0.17}Pb(Br_{0.1}I_{0.9})_3$	Uncoated	No	1.87
$FA_{0.83}Cs_{0.17}Pb(Br_{0.1}I_{0.9})_3$	Uncoated	Yes	2.48
$FA_{0.83}Cs_{0.17}Pb(Br_{0.1}I_{0.9})_3$	PTAA	No	0.17
$FA_{0.83}Cs_{0.17}Pb(Br_{0.1}I_{0.9})_3$	PTAA	Yes	0.89

In order to verify the facile back-transfer of holes from the PTAA layer to iodide-rich phase of the phase-segregated $FA_{0.83}Cs_{0.17}Pb(Br_{0.4}I_{0.6})_3$ layer, we performed PLQY measurements on $FA_{0.83}Cs_{0.17}Pb(Br_{0.1}I_{0.9})_3$ (iodide-rich phase) thin films before any halide segregation had occurred under illumination, and compared to that of $FA_{0.83}Cs_{0.17}Pb(Br_{0.4}I_{0.6})_3$ (mixed phase) from Oliver *et al.*[S11] We note that the mixed phase half-devices from Oliver *et al.* had a ITO/PTAA/PFN/perovskite structure, whilst the iodide-rich half-devices studies by us here had a glass/perovskite/PTAA structure, however we believe such difference will have minimal effects on the PLQY measurements, especially for an order-of-magnitude com-

parison. The measurements were performed under the same conditions. The iodide content of the iodide-rich phase of $FA_{0.83}Cs_{0.17}Pb(Br_{0.4}I_{0.6})_3$ after halide segregation was estimated from the peak energy of $\sim 1.6\,eV$ of the low-energy emission emerging under illumination. The PLQY data with PTAA coating presented in Table S1 show that the relative PLQY decrease upon the introduction of a PTAA layer is much smaller for the iodide-rich MHP ($\sim$ 1 order and 2 orders of magnitude, in iodide-rich MHP and mixed-phase MHP respectively), further corroborating a smaller energy gap between the valence band of the MHP layer and the PTAA, leading to more easier transfer of holes from the PTAA layer into the MHP layer. We note this may also be due to fewer active trap states at the MHP/PTAA interface for the iodide-rich MHP.

6 Time-Resolved Photoluminescence

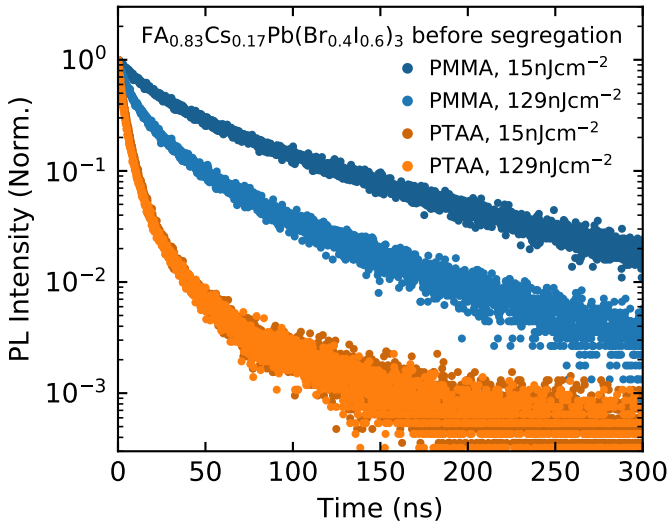

Supplementary Figure S9: Time-resolved PL decay transients for $FA_{0.83}Cs_{0.17}Pb(Br_{0.4}I_{0.6})_3$ thin films without piperidinium ionic additive, coated with either PMMA or PTAA, recorded after halide segregation had occurred under illumination for 150 minutes (470 nm laser with 190 mW cm^{-2} intensity, continuous illumination). Transients were detected at the wavelength corresponding to the low-energy PL from iodide-rich regions (770 nm) following pulsed excitation at 470 nm with two different fluences as shown in the legend.

Time-Resolved photoluminescence (TRPL) collected from the iodide-rich regions of the

PMMA and PTAA-coated $FA_{0.83}Cs_{0.17}Pb(Br_{0.4}I_{0.6})_3$ films without any piperidinium ionic additive, after illumination for 150 minutes, is presented in Figure S9. The PL transients show that the charge-carrier lifetimes are shorter for the PTAA-coated film compared to the PMMA-coated film, in agreement with the TRPL measurement recorded for films before halide segregation had occurred (Figure 3 in the main text).

The halide segregation for TRPL measurements was driven in the XRD/PL setup by a fiber-coupled 470 nm diode laser (PicoQuant LDH-D-C-470, 190 mW cm^{-2} intensity; the same illumination conditions as for the XRD/PL measurements). After the specified illumination time, the segregated film was transferred to the TCSPC sample holder and transients were recorded.

The TRPL transients are usually expected to depend on excitation fluence owing to different recombination mechanisms present and dominating at different charge-carrier concentrations.[S12,S13] Higher fluence usually results in a shorter charge-carrier lifetime because of more significant bimolecular recombination or Auger recombination. Such density-dependent recombination may be approximated by the following rate equation:[S12,S13]

$$\frac{\mathrm{d}n}{\mathrm{d}t} = -k_3 n^3 - k_2 n^2 - k_1 n, \tag{1}$$

where n is the charge-carrier density, k_1 is the monomolecular, trap-mediated recombination rate, k_2 is the bimolecular electron-hole recombination rate, and k_3 is the Auger recombination rate constant. We note however, that trap saturation may lead to time-dependent charge-carrier trapping rates that the above equation is unable to capture.[S14]

As Figure S9 shows, only the PMMA-coated MHP exhibits clear fluence dependence, with such dependence absent for PTAA-coated films. In order to investigate if this absence is due to the low fluence of photoexcitation used for the TRPL measurements, and therefore the charge-carrier recombination still being in the regime where trap-mediated recombination is dominant, we estimated the ratio between trap-mediated recombination rate and radiative

bimolecular recombination rate, given by:

$$\frac{(1/\tau_{\text{bulk}} + 1/\tau_{\text{surf}})n}{k_2 n^2}, \tag{2}$$

where τ_{bulk} and τ_{surf} are charge-carrier lifetimes arising from the bulk and surface recombination. The overall charge-carrier lifetime τ_{eff} and monomolecular recombination rate k_1 is given by:

$$k_1 = \frac{1}{\tau_{\text{eff}}} = \frac{1}{\tau_{\text{bulk}}} + \frac{1}{\tau_{\text{surf}}}. \tag{3}$$

τ_{surf} is given by:[S11]

$$\tau_{\text{surf}} = \frac{d}{\text{SRV}} + \frac{4}{D}\left(\frac{d}{\pi}\right)^2, \tag{4}$$

where d is the effective sample thickness, SRV is the surface recombination velocity, and D is the diffusion coefficient ($D = \mu k_B T/e$, μ is the charge-carrier mobility, k_B is the Boltzmann coefficient, T is the temperature, and e is the elementary charge). We expect the effective sample thickness to be smaller than the sample thickness (both before and after halide segregation) due to the high charge-carrier population near the interface between the MHP and PTAA, as schematically shown in Figure 2 in the main text. We propose that the charge-carrier dynamics within the iodide-rich regions near the interface can be modelled with such smaller effective sample thickness. We plot the ratio given by Equation 2 in Figure S10, using values from Oliver *et al.* ($k_1 = 1 \times 10^7\,\text{s}^{-1}$, $k_2 = 5 \times 10^{-11}\,\text{cm}^3\text{s}^{-1}$, SRV $= 1300\,\text{cms}^{-1}$, $\mu = 32\,\text{cm}^2\text{V}^{-1}\text{s}^{-1}$)[S11] for $129\,\text{nJ}\,\text{cm}^{-2}$ fluence with $2.54 \times 10^{-4}\,\text{cm}^2$ beamsize with varying effective sample thickness. The high value of the recombination ratio across all possible sample thicknesses (Figure S10) demonstrates that PTAA-coated $FA_{0.83}Cs_{0.17}Pb(Br_{0.4}I_{0.6})_3$ is in the recombination regime that is dominated by trap-mediated recombination regardless of the effective thickness, which explains the lack of fluence dependence of PTAA-coated MHP before and after segregation (Figure S11). We however note that this is a simplified picture and estimation to capture the charge-carrier dynamics, especially after halide segregation where we expect small domains, rather than a sheet, of iodide-rich regions to be present

near the interface.

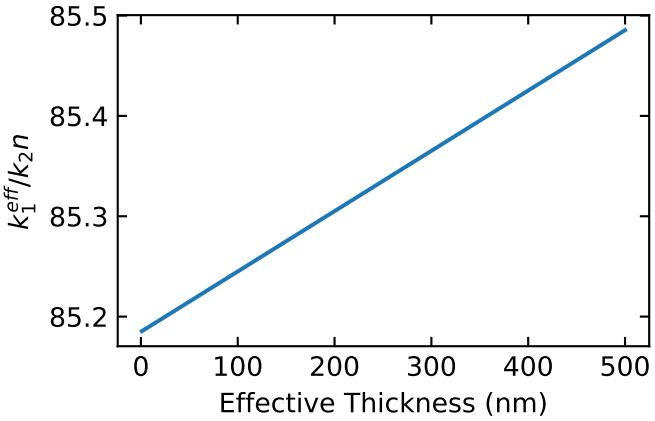

Supplementary Figure S10: Trap-mediated recombination rate / bimolecular recombination rate for PTAA-coated $FA_{0.83}Cs_{0.17}Pb(Br_{0.4}I_{0.6})_3$ under 129 nJ cm^{-2} fluence from a 470 nm pulsed laser with varying effective sample thickness.

6.1 Lifetime Extraction

Charge-carrier lifetimes of the four samples under consideration, $FA_{0.83}Cs_{0.17}Pb(Br_{0.4}I_{0.6})_3$ with or without piperidinium additive, coated with either PMMA or PTAA, were extracted from the TRPL transients before segregation had occurred, as presented in Figure 3 in the main text, and fits are presented in Figure S12. The fits were performed after the initial fast decay had abated, to remove any initial transient effects including charge-carrier trap filling and bimolecular recombination at initial high fluences. The log of the data was fitted to a straight line, corresponding to a monoexponential decay.

The photoluminescence is proportional to the product of the electron (n) and hole (p) densities, and the bimolecular recombination rate (k_2). In an undoped photoexcited semiconductor, the electron and hole populations are equal, and therefore there is a factor of 2 between the charge-carrier recombination rate (k_{cc}) and the PL decay rate (α):

$$\text{PL} \propto k_2 np = k_2 n^2 = k_2 (e^{-k_{cc}t})^2 \propto e^{-\alpha t}, \tag{5}$$

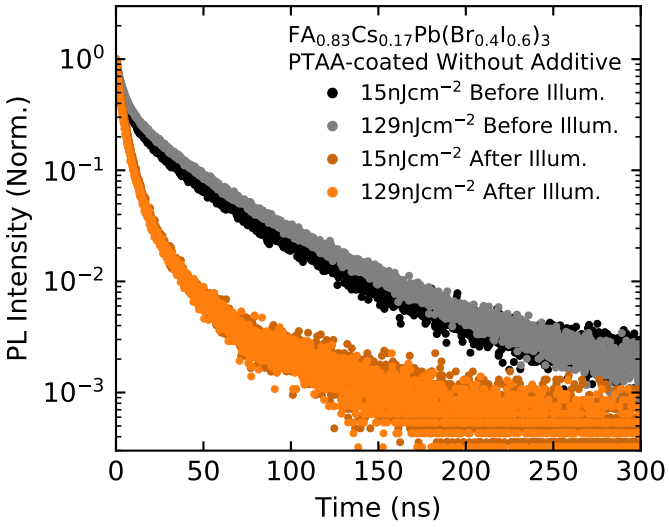

Supplementary Figure S11: Time-resolved PL decay transients for PTAA-coated $FA_{0.83}Cs_{0.17}Pb(Br_{0.4}I_{0.6})_3$ thin films without piperidinium ionic additive, recorded before or after halide segregation had occurred under illumination for 150 minutes (470 nm laser with 190 mW cm^{-2} intensity, continuous illumination). Transients were detected at the wavelength corresponding to the low-energy PL from iodide-rich regions (770 nm) following pulsed excitation at 470 nm with two different fluences as shown in the legend.

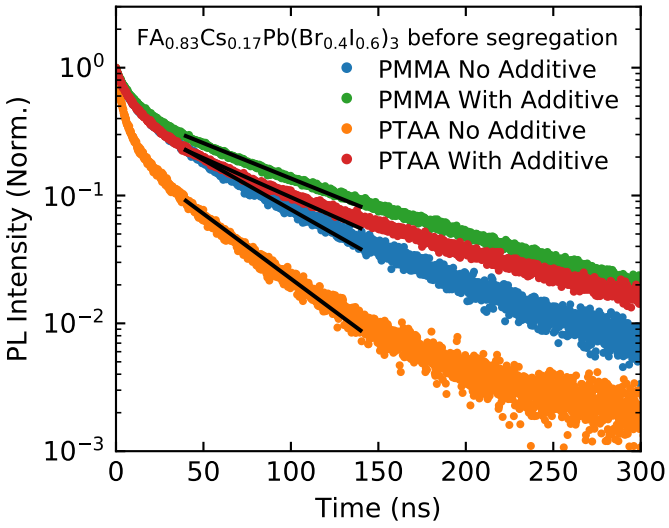

Supplementary Figure S12: PL decay transients of $FA_{0.83}Cs_{0.17}Pb(Br_{0.4}I_{0.6})_3$ thin films with or without piperidinium additive, coated with either PMMA or PTAA. The black lines indicate monoexponential fits. Films were excited with a pulsed laser at 470 nm with fluence of 15 nJcm^{-2} and PL was detected at the high-energy mixed-phase PL (700 nm) before any phase segregation had occurred under illumination.

therefore $2k_{cc} = \alpha$.

The extracted charge-carrier lifetimes are given in Table S2. We note that this does not comprise a full analysis of the transients' shape, but rather serves as a crude indicator of changes to trap-mediated charge-carrier recombination rates upon piperidinium addition, and for different top coating layers. This simplified approach was performed as a quick estimate, rather than a full analysis; further, more rigorous analysis can be found in Ref. S11

Table S2: Extracted charge-carrier lifetimes of the four samples under consideration, $FA_{0.83}Cs_{0.17}Pb(Br_{0.4}I_{0.6})_3$ thin MHP films with or without piperidinium additive, coated with either PMMA or PTAA, extracted from fits assuming monomolecular recombination.

Sample	Charge-carrier lifetime (ns)
MHP without piperidinium additive, PMMA-coated	122
MHP with piperidinium additive, PMMA-coated	157
MHP without piperidinium additive, PTAA-coated	85
MHP with piperidinium additive, PTAA-coated	142

References

(S1) Knight, A. J.; Borchert, J.; Oliver, R. D. J.; Patel, J. B.; Radaelli, P. G.; Snaith, H. J.; Johnston, M. B.; Herz, L. M. Halide Segregation in Mixed-Halide Perovskites: Influence of A-Site Cations. *ACS Energy Lett.* **2021**, *6*, 799–808.

(S2) Tian, Y.; Peter, M.; Unger, E.; Abdellah, M.; Zheng, K.; Pullerits, T.; Yartsev, A.; Sundström, V.; Scheblykin, I. G. Mechanistic Insights into Perovskite Photoluminescence Enhancement: Light Curing with Oxygen Can Boost Yield Thousandfold. *Phys. Chem. Chem. Phys.* **2015**, *17*, 24978–24987.

(S3) Galisteo-López, J. F.; Anaya, M.; Calvo, M. E.; Míguez, H. Environmental Effects on the Photophysics of Organic–Inorganic Halide Perovskites. *J. Phys. Chem. Lett* **2015**, *6*, 2200–2205.

(S4) Motti, S. G.; Gandini, M.; Barker, A. J.; Ball, J. M.; Srimath Kandada, A. R.; Petrozza, A. Photoinduced Emissive Trap States in Lead Halide Perovskite Semiconductors. *ACS Energy Lett.* **2016**, *1*, 726–730.

(S5) Godding, J. S.; Ramadan, A. J.; Lin, Y.-H.; Schutt, K.; Snaith, H. J.; Wenger, B. Oxidative Passivation of Metal Halide Perovskites. *Joule* **2019**, *3*, 2716–2731.

(S6) Yang, Z.; Rajagopal, A.; Jo, S. B.; Chueh, C.-C.; Williams, S.; Huang, C.-C.; Katahara, J. K.; Hillhouse, H. W.; Jen, A. K.-Y. Stabilized Wide Bandgap Perovskite Solar Cells by Tin Substitution. *Nano Lett.* **2016**, *16*, 7739–7747.

(S7) Lin, Y.-H.; Sakai, N.; Da, P.; Wu, J.; Sansom, H. C.; Ramadan, A. J.; Mahesh, S.; Liu, J.; Oliver, R. D. J.; Lim, J.; Aspitarte, L.; Sharma, K.; Madhu, P. K.; Morales-Vilches, A. B.; Nayak, P. K.; Bai, S.; Gao, F.; Grovenor, C. R. M.; Johnston, M. B.; Labram, J. G.; Durrant, J. R.; Ball, J. M.; Wenger, B.; Stannowski, B.; Snaith, H. J. A Piperidinium Salt Stabilizes Efficient Metal-Halide Perovskite Solar Cells. *Science* **2020**, *369*, 96–102.

(S8) de Mello, J. C.; Wittmann, H. F.; Friend, R. H. An Improved Experimental Determination of External Photoluminescence Quantum Efficiency. *Adv. Mater.* **1997**, *9*, 230–232.

(S9) Oliver, R. D.; Lin, Y.-H.; Horn, A. J.; Xia, C. Q.; Warby, J. H.; Johnston, M. B.; Ramadan, A. J.; Snaith, H. J. Thermally Stable Passivation toward High Efficiency Inverted Perovskite Solar Cells. *ACS Energy Lett.* **2020**, *5*, 3336–3343.

(S10) Kirchartz, T.; Márquez, J. A.; Stolterfoht, M.; Unold, T. Photoluminescence-Based Characterization of Halide Perovskites for Photovoltaics. *Adv. Energy Mater.* **2020**, *10*, 1904134.

(S11) Oliver, R. D. J.; Caprioglio, P.; Peña-Camargo, F.; Buizza, L. R. V.; Zu, F.; Ramadan, A. J.; Motti, S. G.; Mahesh, S.; McCarthy, M. M.; Warby, J. H.;

Lin, Y.-H.; Koch, N.; Albrecht, S.; Herz, L. M.; Johnston, M. B.; Neher, D.; Stolterfoht, M.; Snaith, H. J. Understanding and suppressing non-radiative losses in methylammonium-free wide-bandgap perovskite solar cells. *Energy Environ. Sci.* **2022**, *15*, 714–726.

(S12) Herz, L. M. Charge-Carrier Dynamics in Organic-Inorganic Metal Halide Perovskites. *Ann. Phys. Chem.* **2016**, *67*, 65–89.

(S13) Sum, T. C.; Righetto, M.; Lim, S. S. Quo Vadis, Perovskite Emitters? *J. Chem. Phys.* **2020**, *152*, 130901.

(S14) Trimpl, M. J.; Wright, A. D.; Schutt, K.; Buizza, L. R. V.; Wang, Z.; Johnston, M. B.; Snaith, H. J.; Müller-Buschbaum, P.; Herz, L. M. Charge-Carrier Trapping and Radiative Recombination in Metal Halide Perovskite Semiconductors. *Adv. Funct. Mater.* **2020**, *30*, 2004312.